Combustion and Flame 234 (2021) 111640

Contents lists available at ScienceDirect

Combustion and Flame

journal homepage: www.elsevier.com/locate/combustflame

# Analysis of the development of the flame brush in turbulent premixed spherical flames

Tejas Kulkarni*, Fabrizio Bisetti

*Department of Aerospace Engineering and Engineering Mechanics, University of Texas at Austin, Austin, TX 78712, USA*

ARTICLE INFO

*Article history:*
Received 22 April 2021
Revised 21 July 2021
Accepted 22 July 2021

*Keywords:*
Turbulent flame brush
Spherical turbulent flame
Direct numerical simulation

ABSTRACT

The thickness of the turbulent flame brush is central to the modeling of premixed turbulent combustion and the theory of turbulent diffusion is often applied to explain the growth of the brush with varying success. However, numerous studies have shown that the brush evolves differently from the dispersion of material points on the account of flame propagation, density changes across the front, and hydrodynamic instabilities. Modifications to turbulent diffusion theory to incorporate these effects are challenging since the theory is Lagrangian. In this article, we present an alternate Eulerian framework based on the surface density formalism. We employ the proposed framework to analyze a database of direct numerical simulations of spherical turbulent premixed flames in decaying isotropic turbulence and recover mechanisms for which scaling laws are proposed and assessed against data. We characterize quantitatively two mechanisms: one related to the mean velocity gradient induced by thermal expansion and the other due to flame propagation in the presence of curvature. We demonstrate that the net effect of these two processes is to hinder the growth of the turbulent flame brush in the present configuration. Our analysis supports the notion that the turbulent flame brush does not grow indefinitely, rather it attains a maximum thickness.



## 1. Introduction

Burning rates in turbulent premixed flames are several times higher than their laminar counterparts. This enhancement originates from a proportional increase in the flame surface area due to wrinkling by turbulence [1–4].

A quantity central to the modeling of the turbulent flame surface area is the thickness of the flame brush $\delta_T$, which is a statistical measure of the linear extent of the region where the turbulent flame is located over many realizations [5]. In fact, the turbulent flame surface area is related functionally to the standard deviation of the flame surface location around its mean location, which is proportional to $\delta_T$ [4]. The Bray-Moss-Libby model [6] relates the turbulent burning velocity to the product of flame brush thickness and peak density of flame surface area within the brush,

$$S_T/S_L \sim \int_{-\infty}^{\infty} \Sigma \, d\zeta \sim \Sigma_{\max} \delta_T I, \tag{1}$$

where $\Sigma$ is the surface density function, $\zeta$ a local coordinate across the turbulent flame brush, and $I$ a correction factor of order unity.

Apart from its utility in numerical modeling, the flame brush thickness also serves as a characteristic length scale in that the statistics of the reaction progress variable exhibit self-similarity across the turbulent flame brush in a coordinate normalized by $\delta_T$ [7,8]. Examination of the development of the brush is thus essential to turbulent premixed combustion modeling.

The turbulent flame brush is observed to undergo rapid growth in most laboratory and practical combustion devices [9]. Said growth occurs in time for unsteady configurations such as spherical turbulent flames and with distance from the flame holder or injection port for statistically stationary turbulent flames such as Bunsen and V-flames [10–12]. The spatial development of the brush in steady flows may be regarded, at least qualitatively, as temporal development under Taylor's hypothesis [13].

Karlovitz [3] recognized that if the flame propagation speed $S_L$ is small compared to the root mean squared (RMS) velocity fluctuation $u'$, the development of the turbulent flame brush is qualitatively similar to the dispersion of material points in isothermal turbulence. Turbulent diffusion theory [14] relates the dispersion thickness of material points in stationary isotropic turbulence to the Lagrangian velocity auto-correlation function. If an exponential

* Corresponding author.
*E-mail addresses:* tukulkarni@utexas.edu (T. Kulkarni), fbisetti@utexas.edu (F. Bisetti).

https://doi.org/10.1016/j.combustflame.2021.111640
0010-2180/

form is assumed for the auto-correlation function, the dispersion thickness $\tilde{\sigma}$ is given by [15]

$$(\tilde{\sigma}/L_{11})^2 = 2\tilde{t}\left[1 - \frac{1}{\tilde{t}}\left(1 - e^{-\tilde{t}}\right)\right], \tag{2}$$

where $L_{11}$ denotes the transverse correlation length scale and $\tilde{t} = t/\tau^{\dagger}$ the dimensionless time, where the reference time scale $\tau^{\dagger} = L_{11}/u'$ is based on the RMS velocity fluctuation $u'$. Indeed, a qualitative agreement with the short and long time limits of Eq. (2) ($\tilde{\sigma}/L_{11} \sim \tilde{t}$ and $\tilde{\sigma}/L_{11} \sim \tilde{t}^{1/2}$, respectively) was observed in a variety of flame configurations (see Refs. [9,16] and references therein).

If the flame propagation speed is comparable to the RMS velocity fluctuation, the trajectories of flame surface elements are expected to deviate from Lagrangian ones, and a correction is required. Assuming an exponential form of the correlation function, now a function of the ratio $u'/S_L$ also, Scurlock and Grover [4] proposed the following corrections to Eq. (2):

$$(\tilde{\sigma}/l')^2 = 2\frac{t}{\tau'}\left[1 - \frac{\tau'}{t}\left(1 - e^{-t/\tau'}\right)\right], \quad l' = \frac{L_{11}}{1 + S_L/2u'}, \tag{3}$$

and $\tau' = l'/u'$. Goix et al. [17] and Renou et al. [8] applied Eq. (3) successfully to turbulent V-shaped flames and turbulent spherical flames, respectively. However, other experiments [7,18–20] report an increase in $\delta_T$ with increasing $S_L$, while Eq. (3) predicts just the opposite.

In addition to changes in the auto-correlation function due to flame propagation, further deviations from turbulent diffusion theory are expected due to inhomogeneous and anisotropic turbulence, gas expansion due to heat release, and flame propagation in the presence of curvature. Thermal expansion across the reactive front introduces velocity gradients, possibly leading to flame generated turbulence [21,22], which assists in the growth of the brush thickness. Moreover, since the reactant (resp. product) side of the flame brush is predominantly curved convex (resp. concave) towards the reactants, flame propagation serves to reduce the brush thickness through surface destruction in regions of high negative curvature.

Recent experiments in turbulent Bunsen flames have studied the effects of equivalence ratio, background thermodynamic pressure [23], and hydrodynamic instabilities [11] on the evolution of the brush. A robust quantitative model for the development of the turbulent flame brush remains elusive since the turbulent diffusion theory is inherently Lagrangian.

In this article, we present an Eulerian framework based on the surface density formalism. The framework is developed in the context of turbulent spherical flames, but may be extended to other geometries by suitable coordinate transformation to a local coordinate system attached to the flame brush.

The investigation of spherical turbulent flames allows us to assess whether the turbulent flame brush in unsteady configurations grows indefinitely or reaches an asymptotic value in a finite time. A continuous growth of the turbulent flame brush in spherical flames has been reported in experiments [20,24,25], which has been interpreted to indicate that the turbulent burning rates increase monotonically for spherical flames.

The remainder of this article is organized as follows. Section 2 briefly describes the database of direct numerical simulations of pressurized premixed methane/air turbulent spherical flames. A framework for analyzing the turbulent flame brush based on the surface density formalism is established in Section 3. The analysis is presented in Section 4. Section 5 summarizes the results.

## 2. Numerical setup

We consider a set of five direct numerical simulations of spherical flames subjected to freely decaying isotropic turbulence. A brief description of numerical methods and flame configuration follows next. For more details, the reader is directed to our previous work [26].

The unsteady, reactive Navier–Stokes equations are solved in the low Mach number limit with the finite difference solver NGA [27]. Mass conservation is enforced by solving a Poisson equation for the hydrodynamic pressure instead of the continuity equation. The momentum and pressure equations are coupled with a pressure-correction approach [28]. Chemical reactions are modeled with a kinetics mechanism consisting of 16 species and 73 Arrhenius elementary reactions [29]. The integration of the equations for temperature and species mass fractions follows an operator splitting approach in which the convective and diffusive terms are integrated independently of the chemical source terms.

The spatial discretization for the momentum and reactive scalar equations is second order accurate. Convective terms in the scalar equations are treated with the weighted essentially non-oscillatory (WENO) scheme of third order [30]. The time advancement scheme is second order accurate and explicit for the convective terms and implicit for the diffusive and viscous terms. The Poisson equation for the hydrodynamic pressure is solved using the library HYPRE [31]. The system of ordinary differential equations arising from the integration of the chemical sources at each grid point is solved in time by CVODE [32].

The computational domain is a cube with side equal to $2L$ and periodic boundaries in all three directions. A homogeneous grid spacing of $\Delta = 20$ $\mu$m is used for all configurations ensuring adequate resolution of the turbulence spectrum with $\Delta/\eta \leq 0.5$ at all times, where $\eta$ is the Kolmogorov length scale. The grid spacing leads to $\delta_L^0/\Delta = 5.5$, where $\delta_L^0 = (T_u^0 - T_b^0)/\max|\nabla T|$ is the thermal thickness of a laminar flame at the initial conditions. The adequacy of the resolution has been previously demonstrated by Luca et al. [29] for identical thermo-chemical conditions. The simulations feature finite difference grids with $N = 125$ Million (R1) to 8 Billion grid points (R3).

Relevant parameters for the database are listed in Table 1. Four configurations, namely 'R1', 'R2', 'R3' and 'R4', are investigated at increasing ratios of velocity scales $u'/S_L$, length scales $l/\delta_L$, and initial Taylor Reynolds number $\mathrm{Re}_\lambda = u'\lambda/\nu$. Here $l = u'^3/\epsilon$ is the integral length scale based on the RMS velocity fluctuation $u'$ and $\epsilon$, the mean dissipation of the turbulence kinetic energy. Further, $\lambda$ is the Taylor length scale and $\nu$ the kinematic viscosity of the reactants. Additionally, flame 'R3s' features identical conditions as 'R3' but with half the computational domain size to examine the effect of a closed domain.

While increasing the Reynolds number, the Karlovitz number $\mathrm{Ka} = \tau_L/\tau_\eta$ is kept constant. Here $\tau_L = \delta_L/S_L$ and $\tau_\eta = (\nu/\epsilon)^{1/2}$ are the characteristic flame and Kolmogorov time scale, respectively. As a result, the Damköhler number $\mathrm{Da} = (k/\epsilon)/\tau_L \equiv \tau/\tau_L$ increases along with the Reynolds number also. All flames belong to the thin reaction zone regime according to the Borghi-Peters classification of turbulent premixed flames [33].

The simulations are initialized by adding a spherical kernel of burnt gases of radius $R_0$ in fully developed homogeneous isotropic turbulence. The size of the initial kernel relative to an equivalent domain radius $R_L$ is kept approximately the same across the configurations, except for 'R3'. Here, $R_L$ is the radius of a sphere with volume equal to that of the cubic domain, i.e. $R_L = 2L(3/4\pi)^{1/3}$.

The mean radial velocity field evolves as if the computational domain were a sphere of radius $R_L$ [26]. Consistently, the turbulence kinetic energy $k$ in the reactants was obtained by

subtracting the kinetic energy due to mean radial velocity from the total kinetic energy.

The value of the ratio $R_0/R_L$ is chosen such that the initial kernel radius is large compared to the integral velocity length scale $l$, ensuring that the entire turbulence kinetic energy spectrum participates in flame wrinkling from the onset [34].

The turbulent flow field at the onset of the simulations is obtained as follows. First, statistically stationary turbulence at the target Reynolds number is simulated on a smaller cubic periodic domain using a linear forcing scheme [35]. Next, several statistically independent samples of turbulence from the small cubic domain are combined along each direction. Finally, the flow field is advanced by $2\tau_\eta$ to remove discontinuities at the interfaces.

This strategy allows for a large domain compared to the integral length scale as desired. In particular, the ratio of the box half-size to the integral length scale at the onset is $L/l > 20$ for all cases, ensuring a large $R/l$ ratio at all times so that spherical averages consists of many independent samples and statistical convergence is obtained with data from a single simulation.

All pertinent statistics are spherically symmetric and depend on the radial coordinate $r$ and time $t$ only. Using spherical symmetry, statistics are gathered over spherical shells from a single realization of the flow field. Adequate convergence is due to a large $R/l$ ratio, which implies multiple independent and identically distributed samples are collected. This postulate was verified for flame R1 by ensemble averaging four independent simulations.

We observed that the reactant side isotropic turbulence follows a power-law decay [36,37], which for the turbulence kinetic energy $k$ reads

$$k/k_0 = (1 + t/t_0)^{-n} = \exp(-ns), \tag{4}$$

where $n$ and $t_0$ refer to the exponent and the virtual origin of the decay. As shown later, the transformation of the time coordinate $t$ to a logarithmic coordinate $s \equiv \log(1 + t/t_0)$ compensates for the increase in the reference time scale $\tau$. The parameters $n$ and $t_0$ were obtained by least squares fit to the eddy turnover time $\tau = (t + t_0)/n$. The decay exponent $n$ falls in the range $1.55 \le n \le 1.78$, increasing from R1 to R4.

## 3. Mathematical framework

The focus of this study is on the development of the turbulent flame brush, on the mechanisms that affect its growth rate, and on identifying turbulence and flame scales relevant to each of these processes. To this end, we develop a framework based on the surface density formalism. Comparison with the turbulent diffusion theory of Taylor [14] is made where possible.

We identify the instantaneous flame surface as an infinitesimally thin iso-level of the reaction progress variable $C$, which is defined as

$$C \equiv \frac{Y_{O_2} - Y^b_{O_2}}{Y^u_{O_2} - Y^b_{O_2}}. \tag{5}$$

In the above expression, $Y_{O_2}$ denotes to the mass fraction of molecular oxygen and superscripts $u$ and $b$ refer to the unburnt (reactants) and fully burnt (products) states, respectively. In particular, we consider the isolevel $C = c^* = 0.73$, corresponding to the peak conditional heat release rate and thus marking the middle of the reaction layer. Although not shown, all results presented in this article hold over a broad range of isolevels between 0.3 and 0.9. Similarly, other choices for progress variable such as temperature are not expected to affect the results.

The local normal to the flame surface $\boldsymbol{n} = -\nabla C/|\nabla C|$ is defined such that it points towards the reactants ($C = 0$). The flame surface moves in the direction of the normal with a speed $S$ relative to the local fluid velocity [38]

$$S = \frac{1}{|\nabla C|}\frac{DC}{Dt} = \frac{\dot\omega_C}{\rho|\nabla C|} + \frac{\nabla\cdot(\rho\mathbb{D}\nabla C)}{\rho|\nabla C|}, \tag{6}$$

where $D/Dt = \partial/\partial t + \boldsymbol{u}\cdot\nabla$ is the material derivative, $\boldsymbol{u}$ is the local fluid velocity vector, $\mathbb{D}$ the molecular diffusion coefficient, and $\dot\omega_C$ the reaction rate for the progress variable. Computationally, we evaluate the displacement speed as the material derivative (left hand side of Eq. (6)) instead of the sum of the reactive and diffusive components for computational convenience within the confines of the operator-split temporal advancement.

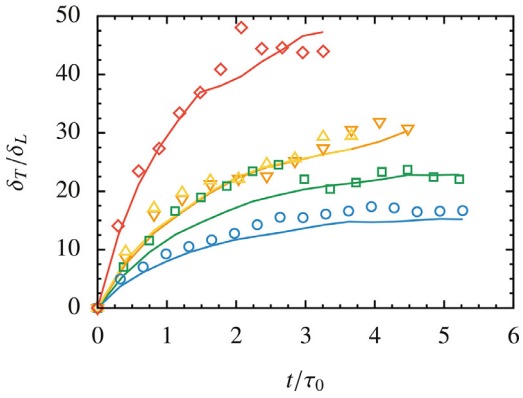


**Fig. 1.** Flame brush thicknesses $\delta_T = \sqrt{2\pi}\sigma$ with $\sigma$ defined as in Eq. (7) (solid lines) and $\widetilde{\delta}_T$ as in Eq. (9) (symbols). For a description of symbols and colors refer to Table 1.

A statistical description of the turbulent spherical flame is considered by recognizing that the radial distance of the flame surface from the center of the domain is a random variable, denoted henceforth by $\phi$. The radial distance $\phi$ of the flame surface follows closely a Gaussian distribution around the mean radial distance. Of particular interest to our analysis is the standard deviation $\sigma$ of the radial distance, defined as

$$\sigma(t) = \left[\int_0^\infty (\varphi - R(t))^2 \mathcal{P}(\phi = \varphi; t)\, d\varphi\right]^{1/2}, \tag{7}$$

where $\mathcal{P}(\phi; t)$ denotes the probability density function (PDF) of the radial distance, $\varphi$ the sample space variable and $R(t)$ the mean radial distance of the flame surface,

$$R(t) = \int_0^\infty \varphi\, \mathcal{P}(\phi = \varphi; t)\, d\varphi. \tag{8}$$

We define the thickness of the flame brush as $\delta_T = \sqrt{2\pi}\sigma$. Inclusion of the factor $\sqrt{2\pi}$ in the definition of $\delta_T$ ensures its consistency with the commonly used definition,

$$\widetilde{\delta}_T = 1/\max\left\{|d\overline{C}/dr|\right\}, \tag{9}$$

where $\overline{C}$ denotes the Reynolds averaged progress variable field. The two definitions are equivalent under the assumption of a Gaussian distribution of the flame surface [16]. Figure 1 demonstrates a good agreement between the two. The former definition will be used in the remainder of this article, since it is less susceptible to statistical noise.

Figure 3 shows two-dimensional planar cuts of the spherical turbulent flame for configuration R4. The region $R - \delta_T/2 \le r \le R + \delta_T/2$ is marked in red hue and contains about 80% of the flame surface area. The turbulent flame brush develops over time and its thickness grows monotonically.

### 3.1. The surface density function

Next, we relate the PDF $\mathcal{P}$ to the surface density function $\Sigma$, which allows us to obtain an ordinary differential equation for $\delta_T$.

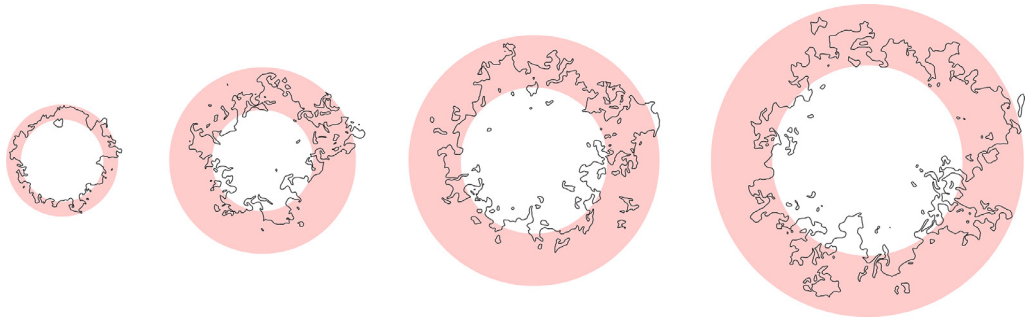

**Fig. 2.** $y-z$ planar slice of the turbulent spherical flame R4. The four snapshots are taken at $t/\tau_0 = 0.3$, 1.2, 2.1, and 3.0 (left to right). The instantaneous flame surface is shown in black color. The shaded red region corresponds to $R-\delta_T/2 \le r \le R+\delta_T/2$, containing about 80% of the total flame surface area.

**Table 1**
Simulation parameters at the initial time. The reference scales refer to flame scales at initial time and are constant across simulations: laminar flame speed $S_L = 1.0$ m/s, thermal thickness $\delta_L = 0.11$ mm, flame time scale $\tau_L = \delta_L/S_L = 0.11$ ms.

| | R1 | R2 | R3 | R3s | R4 |
|---|---|---|---|---|---|
| Symbol | ○ | □ | ▽ | △ | ◇ |
| $N$ | $512^3$ | $1024^3$ | $2048^3$ | $1024^3$ | $1728^3$ |
| $\Delta x$ (μm) | 20 | 20 | 20 | 20 | 20 |
| $R_0/R_L$ | 0.2015 | 0.1511 | 0.1012 | 0.2015 | 0.2015 |
| $u'/S_L$ | 7.4 | 8.5 | 9.8 | 9.8 | 11.21 |
| $l/\delta_L$ | 3.4 | 5.2 | 7.8 | 7.8 | 12.14 |
| $\delta_L/\eta$ | 11.3 | 11.3 | 11.5 | 11.5 | 11.2 |
| $\mathrm{Re}_\lambda$ | 44 | 59 | 77 | 77 | 102 |
| Ka | 25 | 25 | 25 | 25 | 24.4 |
| Da | 0.69 | 0.91 | 1.12 | 1.12 | 1.62 |
| $n$ | 1.55 | 1.57 | 1.58 | 1.72 | 1.78 |

The surface density function is the statistical expectation of the flame surface area per unit volume [39,40]

$$\Sigma(c^*;r,t) = \left\langle |\nabla C| \middle| C = c^* \right\rangle \mathcal{P}_C(C=c^*;r,t). \tag{10}$$

In the equation above, $\mathcal{P}_C$ denotes the PDF of the progress variable and angular brackets indicate statistical expectation. The explicit dependence of the isolevel $C = c^*$ is dropped hereafter for conciseness. By definition, the statistical expectation of the flame surface area $A(t)$ at time $t$ is given by the volumetric integral of the surface density function,

$$A(t) = \int_V \Sigma(\boldsymbol{x},t)\,dV = 4\pi \int_0^\infty r^2 \Sigma(r,t)\,dr. \tag{11}$$

The probability $\mathbb{P}$ that a surface element $dA$ has a radial distance $\phi < \varphi$ is equal to the ratio of the expectation of surface area inside a sphere of radius $\varphi$ to the surface area $A$:

$$\mathbb{P}\{\phi < \varphi\} = A^{-1} \int_0^\varphi 4\pi \xi^2 \Sigma(\xi,t)\,d\xi. \tag{12}$$

Here, $\xi$ is a dummy variable of integration. The probability density function $\mathcal{P}(\phi;t)$ is thus proportional to the surface density function and is given by

$$\mathcal{P}(\phi=\varphi;t) = d\mathbb{P}/d\varphi = 4\pi A^{-1} \varphi^2 \Sigma(r=\varphi,t). \tag{13}$$

Connecting the PDF to the surface density function allows us to obtain its evolution equation as follows. We begin with the surface density transport equation [39,40], simplified to retain only derivatives in $r$ and $t$

$$\frac{\partial \Sigma}{\partial t} + \frac{1}{r^2}\frac{\partial}{\partial r}\left(r^2 \langle (\boldsymbol{u} + S\boldsymbol{n})\cdot \boldsymbol{e}_r \rangle_w \Sigma\right) = \langle K \rangle_w \Sigma, \tag{14}$$

where $\boldsymbol{e}_r = \boldsymbol{x}/||\boldsymbol{x}||$ is the unit vector in the radial direction and $K$ is the flame stretch rate [41]

$$K = \left[ -\boldsymbol{n}^T (\nabla \boldsymbol{u}) \boldsymbol{n} + \nabla \cdot \boldsymbol{u} \right] - 2S\kappa \tag{15}$$

with $\kappa = -(\nabla \cdot \boldsymbol{n})/2$ the flame curvature. The flame stretch rate features contributions from hydrodynamic tangential strain (terms in the square brackets) and flame propagation in the presence of mean surface curvature. In Eq. (14), $\langle . \rangle_w$ denotes the surface weighted average,

$$\langle Q \rangle_w \equiv \frac{\langle Q|\nabla C| \rangle}{\langle |\nabla C| \rangle}. \tag{16}$$

Integrating Eq. (14) over the domain gives the following expression for the logarithmic time rate of change of the expected area

$$\frac{1}{A}\frac{dA}{dt} = \int_0^\infty \frac{4\pi\xi^2\Sigma}{A} \langle K \rangle_w \, d\xi = \int_0^\infty \mathcal{P}(\varphi;t) \langle K \rangle_w \, d\varphi. \tag{17}$$

Since the transport terms integrate to zero, the logarithmic rate of change of the expected area in Eq. (17) is termed *global stretch rate* and denoted henceforth by $K_G = d\ln A/dt$.

Using Eqs. (13), (14) and (17), the rate of change of the PDF is given by

$$\frac{\partial \mathcal{P}}{\partial t} = \frac{4\pi r^2}{A}\left(\frac{\partial \Sigma}{\partial t} - \frac{\Sigma}{A}\frac{dA}{dt}\right) \tag{18}$$

$$= -\frac{\partial}{\partial r}(\langle u_r + Sn_r \rangle_w \mathcal{P}) + \mathcal{P}\langle K' \rangle_w, \tag{19}$$

where $K' = K - K_G$ is the *differential flame stretch rate*. In Eq. (19), the subscript $r$ denotes the radial components of the appropriate vectors, i.e. $u_r = \boldsymbol{u}\cdot\boldsymbol{e}_r$ and $n_r = \boldsymbol{n}\cdot\boldsymbol{e}_r$.

### 3.2. Governing equation for $\delta_T$

An ordinary differential equation for the flame brush thickness $\delta_T$ is obtained by differentiating Eq. (7) with respect to time and substituting into Eq. (19),

$$\frac{d\delta_T}{dt} = \frac{2\pi}{\delta_T}\int_0^\infty \langle u_r' \rangle_w (r-R)\,\mathcal{P}\,dr + \frac{2\pi}{\delta_T}\int_0^\infty \overline{u}_r (r-R)\,\mathcal{P}\,dr + \frac{2\pi}{\delta_T}\int_0^\infty \langle Sn_r \rangle_w (r-R)\,\mathcal{P}\,dr + \frac{\pi}{\delta_T}\int_0^\infty \langle K' \rangle_w (r-R)^2\,\mathcal{P}\,dr. \tag{20}$$

All divergence terms have been dropped using integration by parts. Decomposing the radial velocity field into its unconditional Reynolds average $\overline{u}_r$ and the corresponding fluctuation $u_r' = u_r - \overline{u}_r$ allows us to isolate the effect of changes in density across the front on the development of the flame brush. Note that the surface weighted mean of the Reynolds fluctuation $\langle u_r' \rangle_w$ is not zero.

In order to compare the development of the flame brush and its growth rate across different flames in the database, we consider Eq. (20) in dimensionless form. We choose the instantaneous eddy turnover time $\tau = k/\epsilon$ in the reactants as the reference time

scale in order to account for decaying turbulence. The time derivative $d/dt$ is replaced by the corresponding derivative in the logarithmic time coordinate $s$ with $ds = dt/n\tau$. Consistently, we choose the instantaneous integral scale $l = u'^3/\epsilon$ on the reactants' side as a reference length scale.

The evolution of the normalized flame brush thickness $\hat{\delta}_T \equiv \delta_T/l$ in the logarithmic time coordinate $s$ is given by

$$\frac{d\hat{\delta}_T}{ds} = n\tau\,\frac{d(\delta_T/l)}{dt} = \frac{3n}{2\,u'}\frac{d\delta_T}{dt} - \frac{\delta_T}{l^2}\frac{dl}{ds} \tag{21}$$

$$= \frac{3n}{2\,u'}\frac{d\delta_T}{dt} - (1-n/2)\,\hat{\delta}_T, \tag{22}$$

since $\tau/l = (k/\epsilon)(u'^3/\epsilon)^{-1} = 3/(2u')$ and the integral length scale evolves as $l/l_0 = \exp((1-n/2)s)$. The two terms on the right hand side of the above equation quantify the effect of the growing brush and the evolution of the reference length scale itself.

Substituting for $d\delta_T/dt$ from Eq. (20), we obtain

$$\frac{d\hat{\delta}_T}{ds} = \underbrace{\frac{nC_\delta}{u'}\int_{-R/\sigma}^{\infty}\left\langle u_r'\right\rangle_w\theta\hat{\mathcal{P}}\,d\theta - (1-n/2)\,\hat{\delta}_T}_{\Pi_1} + \underbrace{\frac{nC_\delta}{u'}\int_{-R/\sigma}^{\infty}\overline{u}_r\,\theta\hat{\mathcal{P}}\,d\theta}_{\Pi_2}$$
$$+ \underbrace{\frac{nC_\delta}{u'}\int_{-R/\sigma}^{\infty}\langle Sn_r\rangle_w\,\theta\hat{\mathcal{P}}\,d\theta}_{\Pi_3} + \underbrace{\frac{n\hat{\delta}_T\tau}{2}\int_{-R/\sigma}^{\infty}\left\langle K'\right\rangle_w\theta^2\hat{\mathcal{P}}\,d\theta}_{\Pi_4}, \tag{23}$$

where $C_\delta = 3\sqrt{\pi/2}$ is a constant, $\theta = (r-R)/\sigma$ the normalized flame brush coordinate, and $\hat{\mathcal{P}} = \sigma\mathcal{P}$ the corresponding normalized probability density function. The spatial transformation from $r$ to the brush coordinate $\theta$ attaches the frame of reference to the mean radial location of the flame surface.

In the order that they appear in Eq. (23), the terms account for turbulent dispersion in decaying turbulence (term $\Pi_1$), mean velocity (term $\Pi_2$), flame propagation (term $\Pi_3$), and differential flame stretch (term $\Pi_4$).

Eq. (23) identifies four mechanisms that affect the evolution of turbulent flame brush. Term $\Pi_1$ accounts for turbulent dispersion of flame surface elements in decaying turbulence, much like the dispersion of material points in isotropic turbulence. Apart from turbulent dispersion, any spatial inhomogeneities in the mean radial velocity (term $\Pi_2$) and flame propagation speed (term $\Pi_3$) across the flame brush also contribute to changes in the flame brush thickness. Finally, inhomogeneity in the flame stretch rate across the brush lead to different rates of production of flame surface and affect the PDF $\hat{\mathcal{P}}$ and brush thickness (term $\Pi_4$).

The four terms and their balance are shown for flame configuration R2 in Fig. 3. Turbulent dispersion (term $\Pi_1$) dominates early in the evolution leading to a rapid increase in the thickness of the brush. The contributions from mean velocity (term $\Pi_2$) and differential stretch (term $\Pi_4$) increase in magnitude with time, while that of turbulent dispersion decreases. The contribution of flame propagation to the growth of the brush (term $\Pi_3$) is negligible. As a result, the rate of growth of the turbulent flame brush slows down with time, so that its thickness appears to admit an asymptote or a maximum. The remainder of this article analyzes these mechanisms and the development of the turbulent flame brush, proposing suitable scaling laws whenever possible.

## 4. Results and discussion

### 4.1. Turbulent dispersion

For slow, thin fronts with no gas expansion, the evolution of the turbulent flame brush mimics the dispersion of an ensemble of material elements [3] and follows Taylor's theory of turbulent dispersion [14]. Within the proposed Eulerian framework, the effect of turbulent dispersion is described by $\Pi_1$ (Eq. (23)). This allows us to compare $\Pi_1$ to its equivalent from Taylor's theory after appropriate modifications are made for decaying turbulence and changes to the radial direction along Lagrangian trajectories. These modifications were discussed in detail in our past work [26] and are only briefly summarized below.

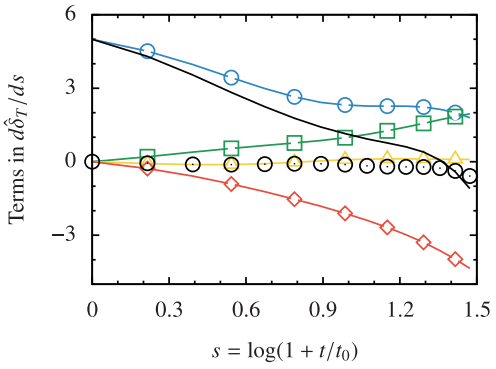


**Fig. 3.** Terms in Eq. (23) for flame R2: turbulent dispersion term $\Pi_1$ (blue circles), mean velocity term $\Pi_2$ (green squares), flame propagation term $\Pi_3$ (yellow triangles), and differential stretch term $\Pi_4$ (red diamonds). Their sum (solid black line) and its difference with respect to the unsteady DNS data (black circles) are also shown. (For interpretation of the references to color in this figure legend, the reader is referred to the web version of this article.)

We consider the evolution of variance of the radial distance $\widetilde{\sigma}^2$ of an ensemble of material elements released at $r = R_0$. For the purpose of comparing against term $\Pi_1$ alone, we consider decaying isotropic turbulence with exponent $n$ and zero mean velocity. Following Taylor [14], the rate of change of $\widetilde{\sigma}^2$ is given by

$$\frac{1}{2}\frac{d\widetilde{\sigma}^2}{dt} = \left\langle\frac{dr(a,t)}{dt}(r(a,t)-R_0)\right\rangle$$
$$= \left\langle\boldsymbol{u}(a,t)\cdot\boldsymbol{e}_r(a,t)\int_0^t\boldsymbol{u}(a,p)\cdot\boldsymbol{e}_r(a,p)\,dp\right\rangle, \tag{24}$$

where $p$ is a dummy variable, $a$ the element index in the ensemble, $\boldsymbol{u}(a,p)$ the local fluid velocity at particle position $\boldsymbol{x}(a,p)$, $r(a,p) = \|\boldsymbol{x}(a,p)\|$ its radial distance, and $\boldsymbol{e}_r = \boldsymbol{x}(a,p)/r(a,p)$ the unit vector in the radial direction. Angular brackets denote averaging over the ensemble.

Simplifying Eq. (24) for isotropic turbulence, we obtain

$$\frac{1}{2}\frac{d\widetilde{\sigma}^2}{dt} = u'(t)\int_0^t u'(p)f_L(p,t)\langle\cos\alpha_{p,t}\rangle\,dp, \tag{25}$$

where $f_L$ denotes the Lagrangian auto-correlation function of the velocity component in any fixed direction $u_x$,

$$f_L(t_1,t_2) \equiv \frac{\left\langle u_x(a,t_1)u_x(a,t_2)\right\rangle}{u'(t_1)\,u'(t_2)}, \tag{26}$$

normalized by the RMS velocity fluctuation $u'$. The orientation factor $\langle\cos\alpha_{p,t}\rangle = \langle\boldsymbol{e}_r(a,p)\cdot\boldsymbol{e}_r(a,t)\rangle$ accounts for changes to the radial direction $\boldsymbol{e}_r$ along Lagrangian trajectories. For a detailed derivation of Eq. (25), the reader is directed to our previous work [26, Appendix B].

Since the orientation factor is less than or equal to unity, the standard deviation of the radial distance is lower than the corresponding dispersion thickness in Cartesian coordinates. A quantitative analysis of the orientation factor requires the simulation of Lagrangian trajectories and is out of the scope of the present work. Instead, we investigate the limiting behavior $\cos\alpha_{p,t} \to 1$ and interpret $\widetilde{\sigma}$ as an upper bound on the standard deviation of the radial distance.

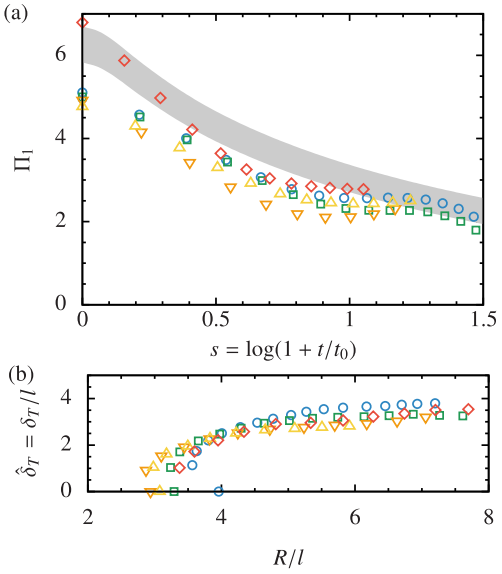


**Fig. 4.** (a) Turbulent dispersion term $\Pi_1$ for different simulations (symbols) against the logarithmic time coordinate $s = \log(1 + t/t_0)$. Comparison with the temporal derivative $d\widehat{\sigma}/ds$ for the range of values $n \in (1.55, 1.78)$, evaluated using Eq. (27) is also shown as a shaded gray area. (b) Normalized turbulent flame brush against the normalized flame radius. Both quantities are normalized by $l$, the instantaneous integral length scale in the reactants. Refer to Table 1 for a description of symbols.

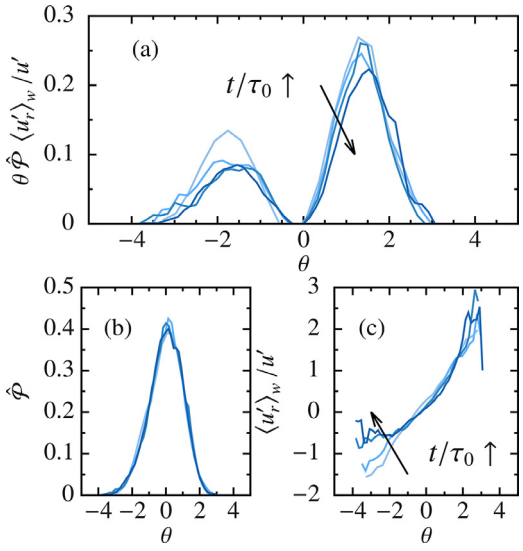


**Fig. 5.** Turbulent dispersion term $\Pi_1$ for simulation R3s: (a) Integrand of the turbulent dispersion term $\theta\,\hat{\mathcal{P}}\,\langle u_r'\rangle_w/u'$ at four instants, (b) PDF of the normalized brush coordinate $\hat{\mathcal{P}} = \sigma\mathcal{P}$, and (c) Normalized gradient weighted radial velocity fluctuation $\langle u_r'\rangle_w/u'$. Simulation time increases in the direction of the arrow, i.e. from light to dark color, corresponding to $t/\tau_0 = 0.81$, 1.63, 2.44, and 3.25.

The self-similarity of the Lagrangian auto-correlation function in freely decaying isotropic turbulence was demonstrated by Huang and Leonard [37]. The two-time Lagrangian auto-correlation function $f_L$ depends only on the lag in the logarithmic time coordinate, $f_L(\Delta s) = f_L(s(t_2) - s(t_1))$. Transforming the temporal derivative in Eq. (25) to that in the logarithmic time coordinate $s$, we obtain

$$\widehat{\sigma}^2 = (9\pi n^2)\int_0^s dp \int_0^p dq\, f_L(q-p)\exp\left\{(1-n/2)(p+q-2s)\right\}, \tag{27}$$

where $p$ and $q$ are dummy variables and $\widehat{\sigma} = \sqrt{2\pi}\widetilde{\sigma}/l$ is the normalized dispersion thickness, consistent with the definition of the turbulent flame brush thickness $\hat{\delta}_T$. The expression for $\widehat{\sigma}$ in Eq. (27) is obtained by using an exponential model for $f_L$ as proposed by Huang and Leonard [37].

The rate of change $d\widehat{\sigma}/ds$ is compared to $\Pi_1$ in Fig. 4(a). The rate of change was evaluated for each configuration using the corresponding value for the decay exponent $n$ and predictions from theory fall in the shaded gray region.

Figure 4 (a) demonstrates that turbulent dispersion is largely similar to the dispersion of material elements for identical turbulence statistics. Term $\Pi_1$ is similar to $d\widehat{\sigma}/ds$, albeit lower in magnitude. The difference likely originates from the orientation factor and deviations from Lagrangian trajectories.

This hypothesis is supported by the following observations. Early on, when the thickness of the turbulent flame brush is small, any movement of flame surface elements in a direction perpendicular to the radial direction is small compared to their radial distance, leading to $\langle\cos\alpha_{p,t}\rangle \approx 1$. Accordingly, we see agreement between term $\Pi_1$ and Eq. (27) at early times. Subsequently, the thickness of the turbulent flame brush grows rapidly compared to the rate of change of the mean radial distance (see Fig. 4(b)), leading to a decreasing orientation factor. In the long time limit, the mean radial distance of the flame surface grows large compared to the thickness of the brush and $\langle\cos\alpha_{p,t}\rangle$ is expected to increase to unity again. The differences between $\Pi_1$ and $d\widehat{\sigma}/ds$ follow this qualitative trend.

We note here that the decrease in the magnitude of $\Pi_1$ in time is not due to the decay of turbulence on the reactants side, since the decay is accounted for by the reference velocity scale $u'$, which changes in time. Instead, the decrease results from the decorrelation of the radial velocity fluctuations in time, consistently with Taylor's theory.

In the Eulerian framework, the decorrelation manifests itself as a decrease in the magnitude of the normalized radial velocity fluctuation $\langle u_r'\rangle_w/u'$, while the distribution of the surface density in the normalized brush coordinate remains virtually identical (see Fig. 5). Flame surface elements that experience higher (resp. lower) radial velocity fluctuations than global mean are transported towards the leading (resp. trailing) edge of the brush. Then, the subsequent decrease in the magnitude of the radial velocity fluctuation with time points to a decaying correlation of the velocity fluctuation at the flame surface as expected.

In summary, the development of the turbulent flame brush due to turbulent dispersion is rather similar to that predicted by Taylor's theory. The contribution of this mechanism to the growth of the flame brush decreases with time due to decorrelation of the radial velocity fluctuation.

### 4.2. Mean velocity gradient term

The development of the flame brush is affected also by the mean velocity field introduced by the propagating turbulent flame and associated density change across the brush. Since the mean radial velocity in the reactants is higher than that in the products, the flame surface closer to the reactants (leading edge) propagates faster than that closer to the products (trailing edge), resulting in the broadening of the brush [42]. In the proposed framework this effect is quantified by $\Pi_2$, which reads

$$\Pi_2 = \int_{-R/\sigma}^{\infty} \frac{nC_\delta \overline{u}_r}{u'}\theta\hat{\mathcal{P}}\,d\theta. \tag{28}$$

We investigate, qualitatively, the dependence of $\Pi_2$ on select configuration parameters. The Reynolds averaged continuity equation, simplified considering spherical symmetry, reads

$$\frac{1}{r^2}\frac{\partial r^2\overline{u}_r}{\partial r} = -\frac{1}{\overline{\rho}}\frac{\partial\overline{\rho}}{\partial t} - \frac{\overline{u}_r}{\overline{\rho}}\frac{\partial\overline{\rho}}{\partial r} - \frac{1}{\overline{\rho}r^2}\frac{\partial r^2\overline{\rho' u_r'}}{\partial r}. \tag{29}$$

Further simplifications are made by adopting the following assumptions. First, the Bray–Moss–Libby [43] model for the mean density $\overline{\rho}$ is employed, so that

$$\overline{\rho}(r,t) \approx \rho_u(1-\overline{C}) + \rho_b\overline{C} = \rho_{u,0}\,(p/p_0)^{1/\gamma}\left[1-(1-1/\zeta)\overline{C}\right]. \tag{30}$$

In the equation above $\rho_u(t)$ and $\rho_b(t)$ denote the time dependent densities of the reactants and products, respectively. The effects of radiation and viscous heating are ignored and the compression of reactants away from the flame front is found to be isentropic, so that the reactant density changes as $\rho_u/\rho_{u,0} = (p/p_0)^{1/\gamma}$. Lastly, the ratio of specific heats $\gamma$ and the density ratio $\zeta = \rho_u/\rho_b$ are assumed to be constant.

With these models, the continuity equation reads

$$\frac{1}{r^2}\frac{\partial r^2\overline{u}_r}{\partial r} = -\frac{1}{\gamma}\frac{d\log(p/p_0)}{dt} - \frac{1}{\overline{\rho}r^2}\frac{\partial r^2\overline{\rho' u_r'}}{\partial r} + \frac{1-1/\zeta}{1-(1-1/\zeta)\overline{C}}\left(\frac{\partial\overline{C}}{\partial t} + \overline{u}_r\frac{\partial\overline{C}}{\partial r}\right). \tag{31}$$

The equation above identifies the contributions of background pressure rise in the closed domain, flame propagation, and turbulent mass flux.

A dimensionless form of the equation above is obtained by transforming the coordinates to $s$ and $\theta$ with $(\partial/\partial s)_\theta = n\tau(\partial/\partial t)_r$ and $(\partial/\partial\theta)_s = \sigma(\partial/\partial r)_t$:

$$(1+\theta\sigma/R)^{-2}\,\frac{\partial(1+\theta\sigma/R)^2(\overline{u}_r/u')}{\partial\theta} = \underbrace{-\frac{\hat{\delta}_T}{nC_\delta\gamma}\frac{\partial\log(p/p_0)}{\partial s}}_{\text{pressure}} \underbrace{-(1+\theta\sigma/R)^{-2}\frac{1}{\overline{\rho}u'}\frac{(1+\theta\sigma/R)^2\overline{\rho' u_r'}}{\partial\theta} - \mathsf{F}(\zeta;\overline{C})\frac{\sigma\overline{\boldsymbol{u}'\cdot\nabla C'}}{u'}}_{\text{turbulent flux}} \underbrace{+\mathsf{F}(\zeta;\overline{C})\frac{\overline{(S/S_L)\,(|\nabla C|\sigma)}}{u'/S_L}}_{\text{flame propagation}}, \tag{32}$$

where $\mathsf{F}(\zeta;\overline{C}) = (1-1/\zeta)/[1-(1-1/\zeta)\overline{C}]$ is the coefficient that scales the gradient weighted displacement speed. The velocity field is normalized by the instantaneous RMS velocity fluctuation $u'$. The spatial and temporal derivatives of mean progress variable are substituted from the Reynolds-averaged progress variable equation (Eq. (6)).

The three source terms in Eq. (32) are labeled 'pressure', 'turbulent flux' and 'flame propagation' and compared for flames R3 (dotted lines) and R3s (solid line with symbols) in Fig. 6. Recall that apart from the domain radius $R_L$ all other flow parameters are identical across the two flames.

We observe that all source terms are approximately the same, indicating that the effect of domain size is negligible. The contribution of flame propagation is greater than those of the other two source terms. We expect the following scaling analysis to hold for spherical flames in an open domain also, since the pressure rise term plays a minor role.

The flame propagation source term in Eq. (32) depends on the mean gradient weighted displacement speed $\overline{S|\nabla C|}$ and is parameterized by the density ratio $\zeta$ through the coefficient $\mathsf{F}(\zeta;\overline{C})$.

We begin by rewriting the scaled gradient weighted speed as:

$$\overline{(S/S_L)|\nabla C|\,\sigma} = (\sigma/S_L)\int_0^1 \left\langle S|\nabla C|\,\middle|\,C=c\right\rangle \mathcal{P}_C(C=c)\,dc = \sigma\int_{0^+}^{1^-}\frac{\langle S(C=c)\rangle_w}{S_L}\,\Sigma(C=c)\,dc, \tag{33}$$

where $\langle.\rangle_w$ denotes the surface weighted average at the iso-level $C=c$. The product of the surface weighted displacement speed and surface density function is integrated over all isolevels $0<c<1$. We exclude the reactants ($c=0$) and products ($c=1$) from the integral, where the gradient of the progress variable equals zero. The explicit dependence of statistics on $r$ and $t$ is dropped for clarity.

Further dividing and multiplying by the peak flame surface density $\Sigma_{\max}(C=c^*;t)$, we obtain

$$\overline{(S/S_L)|\nabla C|\,\sigma} = \Sigma_{\max}\sigma\int_{0^+}^{1^-}\frac{\langle S(C=c)\rangle_w}{S_L}\frac{\Sigma(C=c)}{\Sigma_{\max}}\,dc \sim \Sigma_{\max}\delta_T \sim S_T/S_L. \tag{34}$$

The above scaling relies on self-similar profiles of the surface density function $\Sigma(C=c)/\Sigma_{\max}$ and gradient weighted flame speed $\langle S\rangle_w/S_L$ for all iso-levels $C=c$, independent of time and across different flames (not shown). Note that $\Sigma_{\max}$ is defined at the particular isolevel $C=c^*$ that represents the flame, while Eq. (34) integrates the product of the surface density function and displacement speed over all isolevels.

Since the density ratio $\zeta$ is the same for all flames in the present database, the flame propagation source term and $\Pi_2$ scale as $S_T/u'$. Indeed, large variations in $\Pi_2$ with time disappear when multiplied by the ratio $u'/S_T$ as shown in Fig. 7. Thus, $\Pi_2$ increases

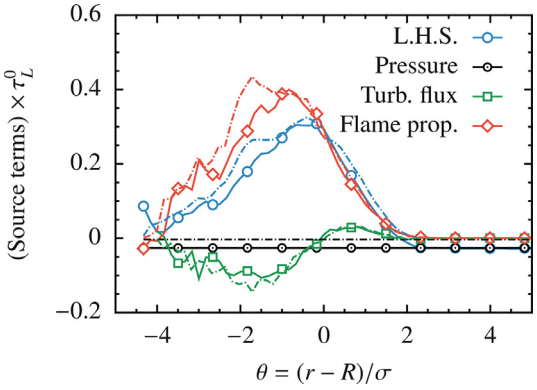


**Fig. 6.** Source terms for the mean radial velocity governing differential equation (Eq. (32)) are shown at $t/\tau_0 = 2.44$. Comparison of source terms for flames R3 (dotted lines) and R3s (solid lines with symbols), showing negligible dependence on domain size.

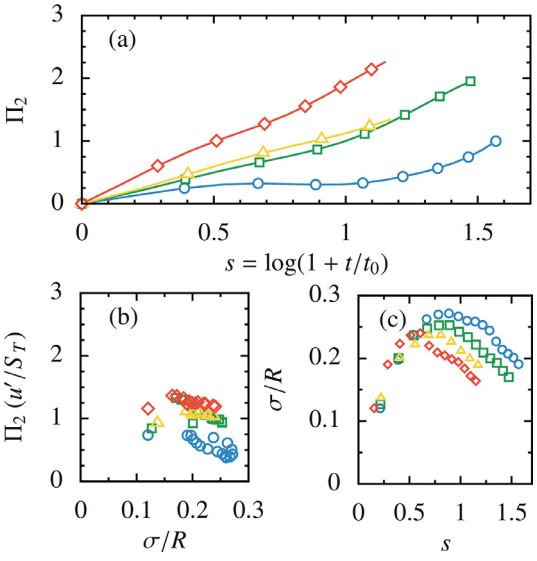


**Fig. 7.** (a) The temporal variation of the mean radial velocity term $\Pi_2$ for all flames. (b) Compensated term $\Pi_2(S_T/u')$ against the parameter $\sigma/R$, (c) Evolution of $\sigma/R$ in time for all flames. Refer to Table 1 for a description of the symbols.

with the turbulent burning rates both in time and across flames R1 to R4.

Eq. (32) suggests that the coefficient $\mathsf{F}(\zeta;\bar{C})$ and mean radial velocity increase with $\zeta$, leading to a faster growth of the brush. While the present database is not suitable for the examination of such dependence, support for this hypothesis comes from recent experiments on turbulent Bunsen and V-shaped flames by Nie et al. [10], Tamadonfar and Gülder [23], and Kheirkhah and Gülder [44]. The researchers report a dependence of the spatial growth rate of the turbulent flame brush on mixture properties and observe deviations from Taylor's theory. We believe that these trends are in part due to mean velocity effects and can be explained qualitatively within our framework, as discussed below.

Tamadonfar and Gülder [23] and Nie et al. [10] report that the growth rate of the flame brush thickness increased when the equivalence ratio changed from 0.7 to 1 for premixed turbulent Bunsen flames of various hydrocarbon fuels. Kheirkhah and Gülder [44] observed a similar increase for turbulent premixed methane/air V-shaped flames. Since the equivalence ratio was changed at fixed turbulence intensity and bulk velocity, it is reasonable to assume that the contribution of the turbulent dispersion mechanism to the development of the brush remained the same.

On the other hand, increases in the equivalence ratio for lean mixtures bring about an increase in the laminar flame speed and density ratio $\zeta$, both of which result in a larger mean velocity gradient across the brush. We note that the modification to the dispersion relation proposed by Scurlock and Grover [4] to account for flame propagation suggests a decrease in the brush thickness with increasing flame speed, contrary to experimental evidence.

Data from Tamadonfar and Gülder [23] for fuel-rich mixtures is consistent with our theory also. The researchers observed that the growth rate decreased when the equivalence ratio increased beyond unity. This trend mimics the dependence of laminar flame speed on equivalence ratio, which peaks near stoichiometry. Moreover, when experiments were repeated at higher turbulence intensity, a lower sensitivity to the equivalence ratio was observed [23,44]. Since a higher turbulence results in a greater relative contribution of turbulent dispersion (term $\Pi_1$) compared to mean velocity (term $\Pi_2$), the lower sensitivity of the turbulent flame brush to equivalence ratio is consistent with our proposition.

In closing, we acknowledge that the mean velocity field and term $\Pi_2$ are geometry dependent. For spherical flames they are influenced by the geometric parameter $\sigma/R$ also (see Eq. (32)). In the limit $\sigma/R \to 0$, the evolution of the flame brush thickness in a spherical configuration is similar to that of a planar flame. This corresponds to both the small time limit ($\sigma \approx 0$) and the long time limit ($R \gg \sigma$). Similar geometry effects are expected in other configurations.

### 4.3. Differential flame stretch

Flame stretch is responsible for production and destruction of flame surface. Since flame stretch varies across the brush, the spatial distribution of flame surface is affected due to unequal rates of production and destruction. In particular, the flame stretch rate changes from negative at the trailing edge (net destruction) to positive at the leading edge (net production). This asymmetry is observed for various turbulent flame configurations and acts to reduce the thickness of flame brush by modifying the spatial distribution of the flame surface. As we discuss below, the change in flame stretch across the brush is primarily associated with that in the flame curvature.

We begin by defining a gradient-weighted displacement speed $S_g \equiv S|\nabla C|/\langle|\nabla C|\rangle$, so that the curvature-propagation component

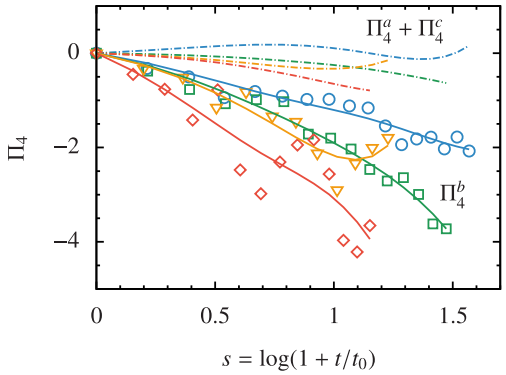


**Fig. 8.** Differential flame stretch terms $\Pi_4^a + \Pi_4^c$ (dot-dashed lines) and $\Pi_4^b$ (symbols and solid lines) in Eq. (23) for all flames in the database. DNS data for $\Pi_4^b$ are shown in symbols, along with a smooth trend-line (lines with same color).

of flame stretch reads

$$\langle S\nabla\cdot\boldsymbol{n}\rangle_w = \frac{\langle S(\nabla\cdot\boldsymbol{n})|\nabla C|\rangle}{\langle|\nabla C|\rangle} = -2\langle S_g\kappa\rangle. \tag{35}$$

Next, the mean of the product $\langle S_g\kappa\rangle$ at the flame surface is further decomposed into the product of the means and a covariance term as

$$-2\langle S_g\kappa\rangle = -2\langle S\rangle_w\langle\kappa\rangle - 2\,\mathrm{covar}\{S_g,\kappa\} = K^b + K^c. \tag{36}$$

Here, the mean curvature $\langle\kappa\rangle$ and covariance are evaluated at the flame surface $C = c^*$, although not indicated explicitly. Note that $\langle S_g\rangle = \langle S\rangle_w$ by definition.

Upon introducing the above definitions, we distinguish between three contributions to flame stretch, i.e. tangential strain $\langle a\rangle_w$, product of mean flame curvature and its displacement speed $K^b$, and their covariance $K^c$. Splitting their contributions to term $\Pi_4$ accordingly, we have

$$\begin{aligned}\Pi_4 &= \Pi_4^a + \Pi_4^b + \Pi_4^c\\ &= \frac{n\tau\hat{\delta}_T}{2}\int_{-R/\sigma}^{\infty}\left(\langle a\rangle_w - K_G^a\right)\theta^2\hat{\mathcal{P}}\,d\theta\\ &\quad + \frac{n\tau\hat{\delta}_T}{2}\int_{-R/\sigma}^{\infty}\left(-2\langle S\rangle_w\langle\kappa\rangle - K_G^b\right)\theta^2\hat{\mathcal{P}}\,d\theta\\ &\quad + \frac{n\tau\hat{\delta}_T}{2}\int_{-R/\sigma}^{\infty}\left(-2\,\mathrm{covar}\{S_g,\kappa\} - K_G^c\right)\theta^2\hat{\mathcal{P}}\,d\theta.\end{aligned} \tag{37}$$

The three contributions to $\Pi_4$ are denoted as $\Pi_4^a$, $\Pi_4^b$, and $\Pi_4^c$, respectively and $K_G^a$, $K_G^b$, and $K_G^c$ are their respective global stretch components:

$$\begin{aligned}K_G^a &= \int_{-R/\sigma}^{\infty}\langle a\rangle_w\hat{\mathcal{P}}\,d\theta, \quad K_G^b = -2\int_{-R/\sigma}^{\infty}\langle S\rangle_w\langle\kappa\rangle\,\hat{\mathcal{P}}\,d\theta,\\ K_G^c &= -2\int_{-R/\sigma}^{\infty}\mathrm{covar}\{S_g,\kappa\}\,\hat{\mathcal{P}}\,d\theta.\end{aligned} \tag{38}$$

Figure 8 shows the three stretch terms $\Pi_4^a$, $\Pi_4^b$ and $\Pi_c^4$ for all flames in the database. The combined contribution of $\Pi_4^a$ and $\Pi_4^c$ is negligible as expected, while $\Pi_4^b$ is greater in magnitude for flames with higher initial Reynolds number, which also have higher initial Damköhler number.

Figure 9 shows the spatial variations of the three stretch components and integrands in terms $\Pi_4^a$, $\Pi_4^b$, and $\Pi_4^c$. The tangential strain rate and the covariance of the displacement speed and curvature are uniform throughout the brush. Since both these terms affect the flame surface uniformly, they do not contribute to the growth of the turbulent brush directly (see Fig. 9(b)).

On the other hand, both the surface-weighted mean displacement speed $\langle S\rangle_w$ and the mean curvature $\langle\kappa\rangle$ vary significantly

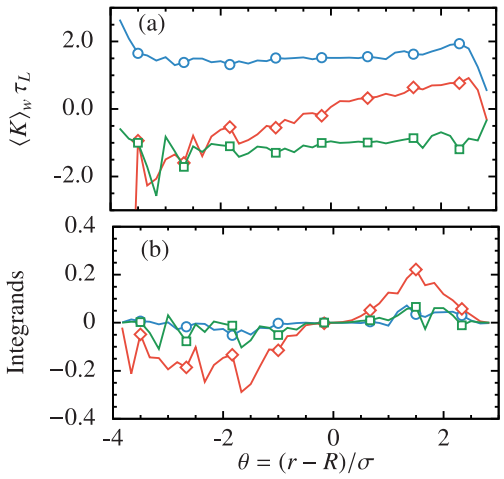


**Fig. 9.** (a) Spatial variation of components of the normalized stretch rate; $\langle a\rangle_w \tau_L$ (blue circles), $-2\langle S_g\rangle\langle\kappa\rangle\tau_L$ (red diamonds), and $-2\,\mathrm{covar}\{S_g,\kappa\}\tau_L$ (green squares). (b) Integrands in terms $\Pi_4^a$, $\Pi_4^b$, and $\Pi_4^c$ in Eq. (37). Stretch components and integrands are normalized by the flame time scale $\tau_L = \delta_L/S_L$. Data shown for flame R3s at time $t/\tau_0 = 2.44$. (For interpretation of the references to color in this figure legend, the reader is referred to the web version of this article)

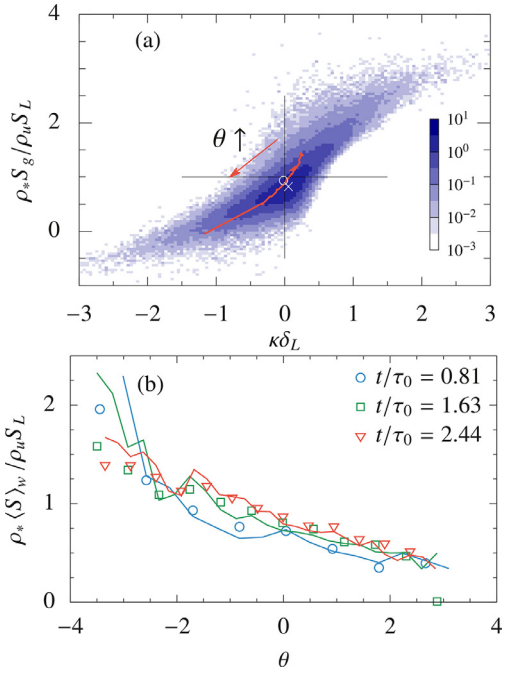


**Fig. 10.** (a) Joint-PDF of $S_g$ and mean curvature $\kappa$. Mean and most probable values are marked with circle and cross, respectively. Red line marks conditional mean of curvature and surface weighted mean of normalized displacement speed at various locations ($-3.5 \le \theta \le 3.5$) across the brush. Arrow marks the direction of increasing $\theta$, i.e. from trailing to leading edge of the brush. Data shown for flame R3s at $t/\tau_0 = 2.44$. (b) Displacement speed across the brush: DNS data (symbols), and predictions from Eq. (41) (lines of same color).

across the brush. Overall, the flame stretch is negative (resp. positive) at the trailing edge (resp. leading edge). This behavior is well documented for spherical [45,46] and planar flames [47,48] and understood to be universal.

That the mean curvature $\langle\kappa\rangle$ itself varies across the brush is a fundamental topological feature of a closed surface; the portion of a closed surface behind (resp. ahead of) its mean location in the direction of the mean normal must necessarily be positively (resp. negatively) curved on average.

Figure 10 (a) presents the joint probability density function of the two at the flame surface (conditioned on $C = c^*$). The displacement speed is multiplied by the ratio of the density $\rho_*$ at $C = c^*$ and $\rho_u$ in a laminar flame to compensate for differences between the displacement speed and the laminar flame speed. The presence of the weight $|\nabla C|/\langle|\nabla C|\rangle$ in $S_g$ de-emphasizes large displacement speeds in highly curved areas at the trailing and leading edges of the brush, where $|\nabla C|/\langle|\nabla C|\rangle \ll 1$. As a result, the joint-PDF of $S_g$ and $\kappa$ is S-shaped as shown in Fig. 10(a) instead of a nearly linear joint-PDF of $S$ and $\kappa$ in spherical flames [49].

The normalized gradient-weighted mean displacement speed $\rho_*\langle S_g\rangle/\rho_u S_L$ averaged on the entire surface is approximately equal to unity as expected. Consistent with the topology of spherical flames, the surface-averaged flame curvature is negative, i.e. convex towards the reactants on average. The most probable values of the curvature however, is positive, indicating that concave topologies (i.e. ridges) are more commonly found.

In general, we observe that the variation of the mean displacement speed across the flame brush is strongly correlated with that of the mean flame curvature. The mean of the two random variable is plotted across the brush as a red curve on top of the joint-PDF. As the curvature distribution shifts from largely-positive at the trailing edge to largely-negative at the leading edge, the conditional mean of the normalized gradient-weighted displacement speed decreases from a value above unity towards zero.

The variation in the mean displacement speed across the brush is consistent with Markstein effects, modeled as [50–52]

$$\langle S\rangle_w = \frac{\rho_u S_L}{\rho_*}\left(1 - \mathrm{Ma}\langle K\rangle_w \tau_L\right) \tag{39}$$

$$= \frac{\rho_u S_L}{\rho_*}\left(1 - \mathrm{Ma}\langle a\rangle_w \tau_L + 2\mathrm{Ma}\frac{\langle S\rangle_w}{S_L}\langle\kappa\rangle\delta_L + 2\,\mathrm{Ma}\tau_L\,\mathrm{covar}\{S_g,\kappa\}\right), \tag{40}$$

where $\mathrm{Ma} = \mathcal{L}/\delta_L$ is the Markstein number and $\mathcal{L}$ the Marstein length, which are mixture properties. The density ratio $\rho_*/\rho_u$ compensates for the differences between the displacement speed and the laminar flame speed. Based on calculations of laminar spherical flames at the same thermo-chemical conditions we find $\mathrm{Ma} = 0.33$.

Isolating $\langle S\rangle_w$ in Eq. (39), we obtain

$$\frac{\rho_*\langle S\rangle_w}{\rho_u S_L} = \left(\frac{1 - \mathrm{Ma}\,\mathrm{Ka}(\langle a\rangle_w - 2\,\mathrm{covar}\{S_g,\kappa\})\tau_\eta}{1 - 2\mathrm{Ma}\,(\rho_u/\rho_*)\langle\kappa\rangle\delta_L}\right). \tag{41}$$

The tangential strain rate $\langle a\rangle_w$ is normalized with the instantaneous Kolmogorov time scale $\tau_\eta$ in accordance with its scaling for the deformation material elements in isotropic turbulence [53]. A similar scaling is also shown to hold in premixed turbulent flames [54,55]. Consistently, we use $\tau_\eta$ to normalize the covariance term also and the Karlovitz number $\mathrm{Ka} = \tau_L/\tau_\eta$ appears in the numerator as a result, although our choice is by no means unique.

Figure 10 (b) shows the variation in the displacement speed across the brush. Data are shown at three different times for flame R3s (symbols) and compared with the predictions of Eq. (41) with $\mathrm{Ma} = 0.33$. A good agreement is observed in the middle of the brush, when flame stretch is small. At the leading and trailing edges of the brush, large curvature leads to large flame stretch and deviations from the linear Markstein model is observed. However, these differences do not affect the integral in $\Pi_4^b$ appreciably since $\hat{\mathcal{P}}\theta^2 \to 0$ at the edges of the brush.

The two stretch components and mean curvature across the brush are shown in Fig. 11. The spatial variation in $\langle S\rangle_w$ at a particular time originates from its dependence on curvature alone, since both the tangential strain rate $\langle a\rangle_w\tau_\eta$ and the covariance stretch $K^c\tau_\eta$ do not change appreciably across the brush. However, according to Eq. (41), they reduce the flame speed $\langle S\rangle_w$ and scale $\Pi_4^b$ indirectly.

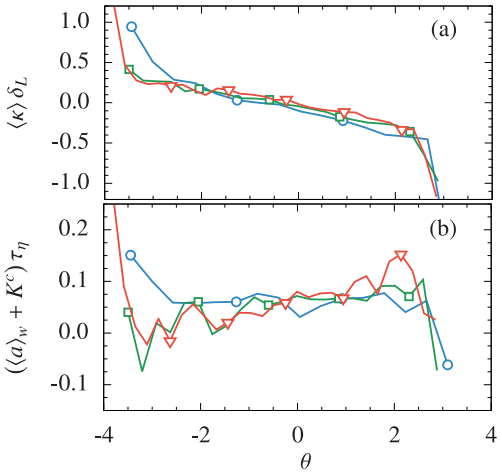


**Fig. 11.** (a) Spatial variation of mean curvature normalized by $\delta_L$. (b) The sum of tangential strain rate $a$ and covariance stretch $K^c = -2\,\mathrm{covar}(S_g, \kappa)$ terms normalized by the instantaneous Kolmogorov time scale $\tau_\eta$. Data shown for flame R3s at $t/\tau_0 = 0.81$ (blue circles), 1.63 (green squares), and 2.44 (red diamonds). (For interpretation of the references to color in this figure legend, the reader is referred to the web version of this article)

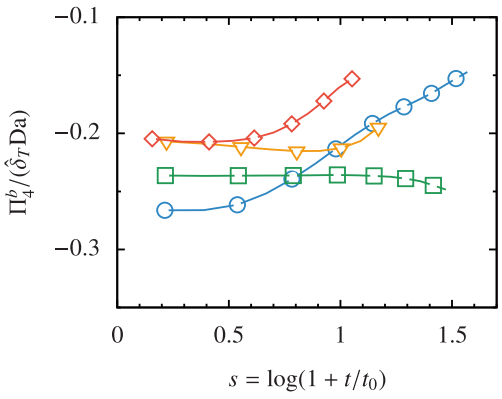


**Fig. 12.** $\Pi_4^b$ compensated by $\hat{\delta}_T$ Da as suggested by Eq. (42). Refer to Table 1 for a description of the symbols.

Substituting $\langle S\rangle_w$ from Eq. (41) in Eq. (37), we obtain

$$\Pi_4^b = -n\hat{\delta}_T\,\mathrm{Da}\int_{-R/\sigma}^{\infty} d\theta\hat{\mathcal{P}}\theta^2 \left(\frac{\rho_u}{\rho_*}\frac{1 - \mathrm{Ma\,Ka}\,\tau_\eta\left(\langle a\rangle_w - 2\,\mathrm{covar}(S_g,\kappa)\right)}{1 - 2\mathrm{Ma}(\rho_u/\rho_*)\langle\kappa\rangle\delta_L}\langle\kappa\rangle\delta_L - K_G^b\tau_L\right), \tag{42}$$

where the Damköhler number $\mathrm{Da} = \tau/\tau_L$ originates from the choice of normalizing scales.

Figure 12 presents term $\Pi_4^b$ normalized by the product $\hat{\delta}_T$Da as suggested by Eq. (42). The normalization seeks to compensate for the temporal variation of $\Pi_4$ due to increasing brush thickness and decreasing Damköhler number. The magnitude of term $\Pi_4^b$ increases in time with the brush thickness itself (Eq. (37)). As with the mean velocity term, flame stretch effects are negligible early on when turbulent diffusion dominates. As the brush grows, the flame stretch term increases and hinders further growth of the brush. However, the magnitude of $\Pi_4$ continues to increase even as the thickness reaches an asymptotic value ($s > 1$ for flame R2). This residual temporal variation may be due to deviations from Markstein theory, variation in the normalized curvature $\langle\kappa\rangle\delta_L$, or other transient effects.

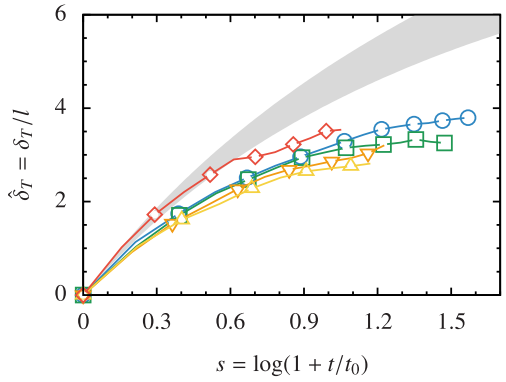


**Fig. 13.** Comparison of the normalized turbulent flame brush thickness $\hat{\delta}_T = \delta_T/l$ for all simulations (lines with symbols). Shaded grey region is bound by the modified isothermal dispersion relation (Eq. (27)) for $n = 1.55$ and $n = 1.78$, the range of values of the decay exponent observed from DNS data.

Overall, the model for $\langle S\rangle_w$ in Eq. (41) highlights the role of the Markstein number in the growth of the flame brush through term $\Pi_4^b$. Since a lower Markstein number leads to a smaller variations of $\langle S\rangle_w$ across the brush, we expect $\Pi_4$ to decrease in magnitude with decreasing Markstein number. While the present database is inadequate to explore such dependence, Fairweather et al. [56] indeed report that methane-hydrogen mixtures with lower Markstein number burn faster than may be attributed to changes in the laminar flame speed alone. Based on the above analysis, we postulate that this might be due to a smaller contribution of $\Pi_4$ towards hindering the growth of the brush. In turn, a thicker brush implies a higher turbulent flame speed.

We note here that Darrieus-Landau (DL) instabilities may affect the flame surface wrinkling and the growth of the flame brush. It has been demonstrated that in the presence of Darrieus-Landau instabilities, the PDF of curvature departs from a Gaussian distribution and exhibits a skewness towards negative curvatures [57]. The accompanying changes to the curvature statistics will affect the stretch terms $\Pi_4^b$ and $\Pi_4^c$ and influence the evolution of the brush. While hydrodynamic instabilities thus may play a role in the evolution of the brush, such effects are minimal in the present configurations due to large values of $u'/S_L$ [26]. Similarly, differential diffusion effects for non-unity Lewis number are expected to change the response of the flame speed to the curvature and affect the flame stretch term.

### 4.4. The growth of the turbulent flame brush

In this article we identified and discussed several mechanisms that control the growth of the flame brush for a spherical turbulent flame. Figure 13 compares the normalized brush thickness $\hat{\delta}_T$ across different flames and against the modified dispersion relation. The dimensional flame brush thickness $\delta_T$ changes by a factor of four from R1 to R4 (see Fig. 1), yet the normalized thickness $\hat{\delta}_T$ evolves similarly across flame configurations. This demonstrates that the integral scale $l$ is the most appropriate normalizing scale for the thickness of the turbulent flame brush, even as turbulence in the reactants decays freely and in the presence of additional mechanisms.

The shaded region in Fig. 13 shows the predictions of the modified turbulent dispersion relation for the range of values of the decay exponent $n$ observed in the database. A better agreement between the two is seen early on as the initial growth of the turbulent brush is governed by turbulent dispersion. More important differences appear as the mean velocity gradient and differential stretch terms grow in magnitude. The normalized turbulent flame brush thickness appears to saturate, contrary to the thickness of

the region occupied by material points, which continues to grow even in decaying isotropic turbulence [37].

A characterization of the various terms points to universal mechanisms that are likely to apply in flame configurations other than the one considered in this study. We observed that the role of turbulent dispersion weakens in time compared to other effects. This decline is due to the decorrelation of the velocity fluctuation experienced by the flame surface elements, consistent with Taylor's theory. Thus, a similar behavior is also expected in statistically stationary homogeneous isotropic turbulence. On the other hand, differential stretch and mean transport become more important as the brush thickness increases because differences in the mean velocity field and stretch rates between the leading and trailing edges are amplified. This is clear as these two mechanisms are proportional to the normalized brush thickness.

Based on the preliminary characterization of expanding turbulent flames from our database, the latter seems to dominate the former. The analysis presented in this article suggests that the thickness of a spherical turbulent flame brush reaches an asymptotic value at which point a balance between turbulent dispersion, mean velocity, and differential stretch terms is attained.

## 5. Conclusions

We developed an Eulerian framework and analyzed the evolution of the turbulent flame brush in spherical turbulent flames subjected to freely decaying isotropic turbulence. The effects of flame propagation, mean velocity and flame stretch were identified.

While the framework based on the surface density function itself is general, we adopted the following assumptions in order to facilitate the task of scaling various terms. To compare term $\Pi_1$ with the theory of turbulent diffusion, changes to the radial direction along Lagrangian trajectories were ignored. A homogeneous isotropic turbulence with no mean flow and shear was considered. Further, we assumed that the flame is sufficiently thin and the Bray-Moss-Libby model for mean density is applicable.

We observed that the early development of the brush occurs primarily due to transport of flame surface elements by turbulence, consistent with the isothermal turbulent diffusion theory of Taylor [14]. Large deviations from this theory appear at later time due to additional effects, which hinder the growth of the brush. As a result, the turbulent flame brush thickness attains a maximum value, in contradiction with turbulent diffusion theory, which predicts indefinite growth. The proposed Eulerian framework explains this behavior and also the dependence of the brush thickness on thermo-chemical parameters, such as equivalence ratio, due to changes in the density ratio. We note that, while modifications to Taylor's theory to account for these effects have been proposed, they show limited success and are generally more difficult to incorporate into a Lagrangian model.

In closing, we remark that more work on select issues is needed in order to generalize our findings on the growth of the turbulent flame brush thickness. First, we considered homogeneous isotropic turbulence fluctuations and the mean velocity was due to flame propagation alone. Practical flow configurations feature both inhomogeneous and anisotropic turbulent fluctuations in the presence of mean shear. Secondly, our choice of mixture and operating conditions is such that both differential diffusion effects and Darrieus-Landau instabilities are suppressed. Influence of these mechanisms on the development of the brush requires further investigation.

## Declaration of Competing Interest

The authors declare that they have no known competing financial interests or personal relationships that could have appeared to influence the work reported in this paper.

## Acknowledgments

This work was supported by the National Science Foundation [grant number 1805921]. Numerical simulations were carried out on the "Shaheen" supercomputer at King Abdullah University of Science and Technology (KAUST); and on the "Stampede2" supercomputer at the Texas Advanced Computing Center (TACC) through allocation TG-CTS180002 under the Extreme Science and Engineering Discovery Environment (XSEDE).

## Supplementary material

Supplementary material associated with this article can be found, in the online version, at doi:10.1016/j.combustflame.2021.111640

## References

[1] G. Damköhler, The effect of turbulence on the flame velocity in gas mixtures, Z. Elektrochem 46 (11) (1940) 601–652. English translation NASA Tech. Mem. 1112
[2] K.I. Shelkin, On combustion in turbulent flow, J. Tech. Phys. 13 (9–10) (1947) 520–530. English translation NASA Tech. Mem. 1110
[3] B. Karlovitz, Open turbulent flames, Symp. (Int.) Combust. 4 (1) (1953) 60–67.
[4] A.C. Scurlock, J.H. Grover, Propagation of turbulent flames, Symp. (Int.) Combust. 4 (1) (1953) 645–658.
[5] J.F. Driscoll, Turbulent premixed combustion: flamelet structure and its effect on turbulent burning velocities, Prog. Energy Combust. Sci. 34 (1) (2008) 91–134.
[6] K. Bray, P.A. Libby, J. Moss, Unified modeling approach for premixed turbulent combustion-part i: general formulation, Combust. Flame 61 (1) (1985) 87–102.
[7] M. Namazian, I. Shepherd, L. Talbot, Characterization of the density fluctuations in turbulent V-shaped premixed flames, Combust. Flame 64 (3) (1986) 299–308.
[8] B. Renou, A. Mura, E. Samson, A. Boukhalfa, Characterization of the local flame structure and the flame surface density for freely propagating premixed flames at various Lewis numbers, Combust. Sci. Technol. 174 (4) (2002) 143–179.
[9] A.N. Lipatnikov, J. Chomiak, Turbulent flame speed and thickness: phenomenology, evaluation, and application in multi-dimensional simulations, Prog. Energy Combust. Sci. 28 (1) (2002) 1–74.
[10] Y. Nie, J. Wang, W. Zhang, M. Chang, M. Zhang, Z. Huang, Flame brush thickness of lean turbulent premixed bunsen flame and the memory effect on its development, Fuel 242 (2019) 607–616.
[11] M. Zhang, A. Patyal, J. Wang, Z. Huang, Darrieus-Landau instability effect on the flame topology and brush thickness for premixed turbulent flames, Appl. Therm. Eng. 158 (2019) 113603.
[12] P. Tamadonfar, Ö. Gülder, Flame brush characteristics and burning velocities of premixed turbulent methane/air bunsen flames, Combust. Flame 161 (12) (2014) 3154–3165.
[13] G.I. Taylor, Statistical theory of turbulence, Proc. R. Soc. Lond. Ser. A 151 (873) (1935) 421–444.
[14] G.I. Taylor, Diffusion by continuous movements, Proc. R. Soc. Lond. Ser. A 2 (1) (1922) 196–212.
[15] J.O. Hinze, Turbulence, McGraw-Hill, New York, 1975.
[16] A. Lipatnikov, Fundamentals of Premixed Turbulent Combustion, CRC Press, 2012.
[17] P. Goix, P. Paranthoen, M. Trinite, A tomographic study of measurements in a V-shaped H2-air flame and a lagrangian interpretation of the turbulent flame brush evolution, Combust. Flame 81 (3–4) (1990) 229–241.
[18] A. Boukhalfa, I. Gökalp, Influence of the Damköhler number on the average thickness of conical turbulent premixed methane/air flames, Combust. Flame 73 (1) (1988) 75–87.
[19] J.H. Grover, E.N. Fales, A.C. Scurlock, Turbulent flame studies in two-dimensional open burners, Symp. (Int.) Combust. 9 (1) (1963) 21–35.
[20] S. Kwon, M.-S. Wu, J.F. Driscoll, G.M. Faeth, Flame surface properties of premixed flames in isotropic turbulence: measurements and numerical simulations, Combust. Flame 88 (2) (1992) 221–238.
[21] A. Gulati, J.F. Driscoll, Velocity-density correlations and favre averages measured in a premixed turbulent flame, Combust. Sci. Technol. 48 (5–6) (1986) 285–307.
[22] A.N. Lipatnikov, W.Y. Li, L.J. Jiang, S.S. Shy, Does density ratio significantly affect turbulent flame speed? Flow Turbul. Combust. 98 (2017) 1153–1172.

[23] P. Tamadonfar, Ö.L. Gülder, Effects of mixture composition and turbulence intensity on flame front structure and burning velocities of premixed turbulent hydrocarbon/air bunsen flames, Combust. Flame 162 (12) (2015) 4417–4441.
[24] V.P. Karpov, E.S. Severin, Turbulent burn-up rates of propane-air flames determined in a bomb with agitators, Combust. Explos. Shock Waves 14 (2) (1978) 158–163.
[25] U. Bielert, M. Klug, G. Adomeit, Application of front tracking techniques to the turbulent combustion processes in a single stroke device, Combust. Flame 106 (1) (1996) 11–28.
[26] T. Kulkarni, R. Buttay, M.H. Kasbaoui, A. Attili, F. Bisetti, Reynolds number scaling of burning rates in spherical turbulent premixed flames, J. Fluid Mech. 906 (2021) A2.
[27] O. Desjardins, G. Blanquart, G. Balarac, H. Pitsch, High order conservative finite difference scheme for variable density low mach number turbulent flows, J. Comput. Phys. 227 (15) (2008) 7125–7159.
[28] A.J. Chorin, Numerical solution of the Navier-Stokes equations, Math. Comput. 22 (1968) 745–762.
[29] S. Luca, A.N. Al-Khateeb, A. Attili, F. Bisetti, Comprehensive validation of skeletal mechanism for turbulent premixed methane-air flame simulations, J. Propuls. Power 34 (2018) 153–160.
[30] X.D. Liu, S. Osher, T. Chan, Weighted essentially non-oscillatory schemes, J. Comput. Phys. 115 (1994) 200–212.
[31] R.D. Falgout, J.E. Jones, U.M. Yang, The design and implementation of Hypre, a library of parallel high performance preconditioners, Numerical Solution of Partial Differential Equations on Parallel Computers, Springer (2006), pp. 267–294.
[32] A.C. Hindmarsh, P.N. Brown, K.E. Grant, S.L. Lee, R. Serban, D.E. Shumaker, C.S. Woodward, SUNDIALS: suite of nonlinear and differential/algebraic equation solvers, ACM Trans. Math. Softw. 31 (2005) 363–396.
[33] N. Peters, The turbulent burning velocity for large-scale and small-scale turbulence, J. Fluid Mech. 384 (1999) 107–132.
[34] S. Chaudhuri, V. Akkerman, C.K. Law, Spectral formulation of turbulent flame speed with consideration of hydrodynamic instability, Phys. Rev. E 84 (2) (2011) 026322.
[35] C. Rosales, C. Meneveau, Linear forcing in numerical simulations of isotropic turbulence: physical space implementations and convergence properties, Phys. Fluids 17 (9) (2005) 095106.
[36] G.K. Batchelor, A.A. Townsend, Decay of isotropic turbulence in the initial period, Proc. R. Soc. Lond. Ser. A 193 (1035) (1948) 539–558.
[37] M.J. Huang, A. Leonard, Velocity autocorrelations of decaying isotropic homogeneous turbulence, Phys. Fluids 7 (10) (1995) 2455–2464.
[38] T. Echekki, J.H. Chen, Unsteady strain rate and curvature effects in turbulent premixed methane-air flames, Combust. Flame 106 (1) (1996) 184–202.
[39] S.B. Pope, The evolution of surfaces in turbulence, Int. J. Eng. Sci. 26 (5) (1988) 445–469.
[40] L. Vervisch, E. Bidaux, K. Bray, W. Kollmann, Surface density function in premixed turbulent combustion modeling, similarities between probability density function and flame surface approaches, Phys. Fluids 7 (10) (1995) 2496–2503.
[41] S.M. Candel, T. Poinsot, Flame stretch and the balance equation for the flame area, Combust. Sci. Technol. 70 (1990) 1–15.
[42] I. Ahmed, N. Swaminathan, Simulation of spherically expanding turbulent premixed flames, Combust. Sci. Technol. 185 (10) (2013) 1509–1540.
[43] K.N.C. Bray, J.B. Moss, A unified statistical model of the premixed turbulent flame, Acta Astronaut. 4 (3–4) (1977) 291–319.
[44] S. Kheirkhah, Ö.L. Gülder, Topology and brush thickness of turbulent premixed V-shaped flames, Flow Turbul. Combust. 93 (3) (2014) 439–459.
[45] S.S. Shy, W.K. I, E.I. Lee, T.S. Yang, Experimental analysis of flame surface density modeling for premixed turbulent combustion using aqueous autocatalytic reactions, Combust. Flame 118 (4) (1999) 606–618.
[46] S.S. Shy, E.I. Lee, N.W. Chang, S.I. Yang, Direct and indirect measurements of flame surface density, orientation, and curvature for premixed turbulent combustion modeling in a cruciform burner, Proc. Combust. Inst. 28 (1) (2000) 383–390.
[47] A. Trouvé, T. Poinsot, The evolution equation for the flame surface density in turbulent premixed combustion, J. Fluid Mech. 278 (1994) 1–31.
[48] N. Chakraborty, R.S. Cant, Effects of strain rate and curvature on surface density function transport in turbulent premixed flames in the thin reaction zones regime, Phys. Fluids 17 (6) (2005) 065108.
[49] K.W. Jenkins, M. Klein, N. Chakraborty, R.S. Cant, Effects of strain rate and curvature on the propagation of a spherical flame kernel in the thin-reaction–zones regime, Combust. Flame 145 (1) (2006) 415–434.
[50] N. Peters, Turbulent Combustion, IOP Publishing, 2001.
[51] P. Pelce, P. Clavin, Influence of hydrodynamics and diffusion upon the stability limits of laminar premixed flames, J. Fluid Mech. 124 (1982) 219–237.
[52] M. Matalon, B.J. Matkowsky, Flames as gasdynamic discontinuities, J. Fluid Mech. 124 (1982) 239–259.
[53] S.S. Girimaji, S.B. Pope, Material-element deformation in isotropic turbulence, J. Fluid Mech. 220 (1990) 427–458.
[54] S. Luca, A. Attili, E.L. Schiavo, F. Creta, F. Bisetti, On the statistics of flame stretch in turbulent premixed jet flames in the thin reaction zone regime at varying reynolds number, Proc. Combust. Inst. 37 (2) (2019) 2451–2459.
[55] T. Kulkarni, F. Bisetti, Evolution and scaling of the peak flame surface density in spherical turbulent premixed flames subjected to decaying isotropic turbulence, Proc. Combust. Inst. 38 (2) (2021) 2817–2824.
[56] M. Fairweather, M. Ormsby, C. Sheppard, R. Woolley, Turbulent burning rates of methane and methane-hydrogen mixtures, Combust. Flame 156 (4) (2009) 780–790.
[57] F. Creta, R. Lamioni, P.E. Lapenna, G. Troiani, Interplay of Darrieus-Landau instability and weak turbulence in premixed flame propagation, Phys. Rev. E 94 (5-1) (2016) 053102.